The strength of sintered and adhesively bonded zirconia/veneer-ceramic bilayers

Costa, Anna Karina F; Borges, Alexandre Luiz S; Fleming, Garry James P; Addison, Owen

DOI:
10.1016/j.jdent.2014.08.001

License:
Other (please specify with Rights Statement)

Document Version
Peer reviewed version

Citation for published version (Harvard):
Costa, AKF, Borges, ALS, Fleming, GJP & Addison, O 2014, 'The strength of sintered and adhesively bonded zirconia/veneer-ceramic bilayers', *Journal of Dentistry*, vol. 42, no. 10, pp. 1269-1276. https://doi.org/10.1016/j.jdent.2014.08.001

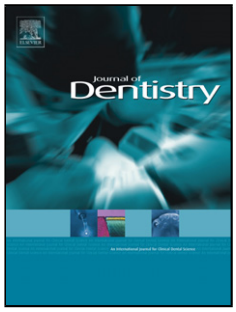

Title: The strength of sintered and adhesively bonded zirconia/veneer-ceramic bilayers

Author: Anna Karina F. Costa Alexandre Luiz S. Borges Garry James P Fleming Owen Addison

PII: S0300-5712(14)00235-8
DOI: http://dx.doi.org/doi:10.1016/j.jdent.2014.08.001
Reference: JJOD 2339

To appear in: *Journal of Dentistry*

Received date: 16-5-2014
Revised date: 10-7-2014
Accepted date: 7-8-2014

Please cite this article as: Costa AKF, Borges ALS, Fleming GJP, Addison O, The strength of sintered and adhesively bonded zirconia/veneer-ceramic bilayers, *Journal of Dentistry* (2014), http://dx.doi.org/10.1016/j.jdent.2014.08.001

The strength of sintered and adhesively bonded zirconia/veneer-ceramic bilayers

Anna Karina F. Costa[1,2], Alexandre Luiz S. Borges[2], Garry James P Fleming[3] and Owen Addison[1]

[1]Biomaterials Unit, University of Birmingham School of Dentistry, St. Chad's Queensway, Birmingham B4 6NN, UK,

[2]Dental Materials and Prosthodontics Unit, Sao Jose dos Campos Dental School, Institute of Technology and Science, SP, Brazil

[3]Materials Science Unit, Dublin Dental University Hospital, Lincoln Place, Dublin 2, Republic of Ireland

Keywords: CAD-CAM, bi-axial flexure strength, zirconia, veneer-ceramic, fracture, FEA, fractography.

Corresponding Author: Owen Addison,
Biomaterials Unit,
University of Birmingham School of Dentistry,
St. Chad's Queensway,
Birmingham,
United Kingdom.

Telephone: 00 44 121 466 5506

E-Mail: addisono@adf.bham.ac.uk

ABSTRACT

Objectives: Recently all-ceramic restorative systems have been introduced that use CAD/CAM technology to fabricate both the Y-TZP core and veneer-ceramic layers. The aim was to identify whether the CAD/CAM approach resulted in more favourable stressing patterns in the veneer-ceramic when compared with a conventionally sintered Y-TZP core/veneer-ceramic.

Methods: Nominally identical Vita VM9 veneer-ceramic disc-shaped specimens (0.7 mm thickness, 12 mm diameter) were fabricated. 20 specimens received a surface coating of resin-cement (Panavia 21); 20 specimens were bonded with the resin-cement to fully sintered Y-TZP (YZ Vita Inceram Vita) discs (0.27 mm thickness, 12 mm diameter). A final series of 20 Y-TZP core/veneer-ceramic specimens were manufactured using a conventional sintering route. Biaxial flexure strength was determined in a ball-on-ring configuration and stress at the fracture origin calculated using multilayer closed-form analytical solutions. Fractography was undertaken using scanning electron microscopy. The experimental test was simulated using Finite Element Analysis. Group mean BFS were compared one-way ANOVA and post-hoc Tukey test 95% significance level.

Results: Resin cement application resulted in significant strengthening of the veneer-ceramic and further significant strengthening of the veneer-ceramic ($p<0.01$) occurred following bonding to the Y-TZP core. The BFS calculated at the failure origin for conventionally sintered specimens was significant reduced when compared with the adhesively bonded Y-TZP/veneer-ceramic.

Conclusions: Under the test conditions employed adhesive cementation between CAD/CAM produced Y-TZP/veneer-ceramic layers appears to offer the potential to induce more favourable stress states within the veneer-ceramic when compared with conventional sintered manufacturing routes.

INTRODUCTION

Fractographic analysis of failed clinical restorations [1,2] and *in-vitro* simulations have demonstrated that fracture in Y-TZP/veneer-ceramic systems occurs predominantly due to chipping within the veneer-ceramic and/or delamination from the underlying Y-TZP core [3-8]. It has been further shown that the initial flaw can extend sub-critically in areas of high stress concentration which are often in the proximity of a contact load [9]. Sub-critical crack growth in veneer-ceramics is well characterised [10] and is likely to be influenced by the mechanical variables of the masticatory challenge and by the physiochemical characteristics of the oral environment. The rate of crack-extension and to some extent the crack direction will however be modified by the presence and characteristics of residual stress states that exist within the ceramic body [11]. Residual stress states in Y-TZP/veneer-ceramic systems may be introduced during veneer-ceramic sintering as a consequence of the thermal expansion mismatch between the two materials [1,12,13] and as tempering stresses associated with temperature gradients during cooling [14-16]. Residual stresses have the capacity to be both beneficial when manifested as compressive stress states and deleterious as tensile stress states, particularly when located in a region of stress concentration that occurs on application of external load [17]. Consequently considerable focus exists on the development of material, design and processing solutions to optimise residual stress states within Y-TZP/veneer-ceramic systems with the overall aim of decreasing the incidence of fatigue related fracture events.

Traditionally Y-TZP cores are milled in either partially or fully sintered states prior to manual application of an aesthetic veneer-ceramic through a conventional powder condensation and sintering route. To reduce operator variability associated with the manual application/condensation of the veneer-ceramic, commercial Computer-Aided Design/Computer-Aided Manufacture (CAD/CAM) systems have been introduced which fabricate both the core and veneer layers individually -a process which has been described as Rapid Layer Manufacture (RLM) [18]. The two RLM layers are subsequently joined using an interface adhesive comprised of either a low-fusing glass ceramic [19,20] or a resin-cement [18, 21]. The technique has a number of proposed advantages which include a reduced need to match the coefficients of thermal expansion of the two layers which is essential in traditional ceramic fusion manufacture.

When a resin-cement interface adhesive is used the residual stresses introduced by the volumetric shrinkage of the resin-cement would be expected to be insignificant when compared with the thermally introduced stresses associated with conventionally sintered Y-TZP/veneer-ceramic systems [9]. In addition the presence of a thin intermediate layer of resin-cement has also been proposed to provide an internal barrier to crack propagation across and between layers at the interface thereby preventing delamination [22]. Resin-cements have also been shown to have a highly significant interaction with veneer-ceramic surface defects, potentially conferring reinforcements in excess of 100% of the measured system strength [23, 24]. Studies on resin-cementation of monolithic dental ceramics have shown that the reinforcement is sensitive to cement thickness and elastic modulus which can lead to a variation in the critical load for veneer fracture [23, 24].

Investigations into the benefits of RLM when compared with traditional veneer-ceramic sintering routes are limited. Finite Element Analysis (FEA) approaches offer insight into the effect of design variables on stress distributions and fractographic studies can identify fracture origins and patterns. However, it is also important to understand how strength limiting defect populations; thermally introduced stresses and interface variables impact on the system strength. Discerning the contribution of individual components is extremely complex, however, the combined influence may be indirectly assessed by calculating differences in the stress required to initiate fracture at regions within the veneer-ceramic layer where strength modifying variables exist. The current study uses multilayer analytical solutions in combination with bi-axial flexure testing of idealised specimen geometries designed to initiate tensile crack extension in regions of the veneer-ceramic influenced by interfacial and residual stress variables. Given the limited evidence regarding RLM and its potential advantages, the null hypothesis that there would be no difference between the failure stresses in adhesively bonded or sintered veneer-ceramic layers was tested.

MATERIALS AND METHODS

Veneer-ceramic sample preparation

0.6 g of Vita VM9 veneer-ceramic dentine powder was proportioned and manipulated with 0.22 mL of Vita Modelling Fluid (Vita, Bad Sackingen, Germany) to form a reproducible slurry. The slurry was transferred into a plastic ring mould (14 mm diameter x 0.9 mm thickness) which was firmly secured to a flat aluminium base-plate. The slurry was condensed using a vibrating plate and absorbent tissue to remove excess Modelling Fluid. The condensed disc-shaped specimens were then vacuum-fired (Vita Vacumat 40T, Vita Zahnfabrik, Bad Sackingen, Germany) (pre-heated to dry the specimen at 500 °C for 360 s before the temperature was increased at 55 °C/min to 910 °C under vacuum) and air-cooled to room temperature. Following firing the resultant discs with final dimensions of 13 mm diameter x 0.70 ± 0.03 mm thickness were visually inspected and then stored in a desiccator prior to usage.

Y-TZP core-ceramic preparation

Partially sintered Y-TZP CAD/CAM blocs (55 x 19 x 15.5 mm, YZ Vita Inceram Vita, Bad Sackingen, Germany) were rounded to a 15 mm diameter cylinder using a core drill and copious lubricant. The cylinders were then sectioned using a low-speed saw to produce discs. The discs were then manually polished on one surface using a P320 grit silicon carbide abrasive followed by a P500 grit to produce a final pre-sintered thickness of 0.30 ± 0.01 mm. The discs were sintered in Vita ZYRCOMAT 6000 MS Sintering Furnace (Vita Zahnfabrik, Bad Sackingen, Germany) resulting in a final diameter and thickness of 12 mm and 0.27 ± 0.02 mm, respectively. One surface of each Y-TZP disc was then air-abraded (Basic Master- Renfert,

Germany) with 50 μm alumina particles at a pressure of 4 bar from a 2 mm distance for 10 s with the particle incidence angle maintained at 90°. Specimens were washed in copious water and dried in an oil free air stream and stored in a dessicator prior to testing [25].

Sample preparation for biaxial flexure strength (BFS) determination.

Sixty VM9 veneer-ceramic samples were prepared and the surface of each disc that was in contact with the aluminium base-plate during condensation was subsequently etched with 9.6% hydrofluoric (HF) acid (Pulpdent Porcelain Etch Gel, MA, USA) for 60 s then rinsed thoroughly in water and dried. The etched specimens were randomly allocated to three groups (n=20) with specimens from Group A (Figure 1) receiving no further treatment (uncoated control). A further 20 specimens from Group B were silane coated (Rely-X Ceramic Primer, 3M ESPE) for 60 s prior to air drying. Subsequently a layer of chemically-cured resin-cement was applied (Panavia 21, Kuraray Co., Ltd., Tokyo, Japan). The resin-cement was hand-mixed and applied to the centre of the silane primed surface. An acetate film was gently pressed until the resin-cement spread to the disc edges following which the disc was inverted and loaded on a flat surface with 100 g for 10 min.

A further 20 specimens (Group C) were also silane primed and then resin-cemented to the air-abraded Y-TZP surface creating a bilayer in a process mimicking RLM. A quantity of resin-cement was applied to the centre of the veneer-ceramic disc surface prior to inverting the disc onto the Y-TZP and loading with 100 g for 10 min. Excess resin-cement was carefully removed from the sample periphery. To compare RLM with a traditional veneer-ceramic condensation process, 20 additional specimens (Group D) were prepared by manipulating the VM9 veneer-

ceramic slurry onto the air abraded Y-TZP disc-shaped specimen surface which was positioned in a 1.2 mm thickness ring mould. Following vibration condensation to remove the excess modelling liquid, specimens were vacuum-fired (identical firing sequence to specimens from Groups A-C) and air-cooled to room temperature. The geometries of samples prepared for Groups A-D are demonstrated in figure 1.

BFS testing.

The BFS was determined in a ball-on-ring configuration using a cross-head speed of 1 mm/min at a room temperature of 23 ±1 °C. To provide a consistent flat loading surface the upper surfaces of all samples (Groups A-D) were gently hand-polished with P320 and P500 silicon carbide abrasives. The upper surface was then centrally loaded with a 4 mm diameter spherical stainless steel ball indenter whilst the lower surface (HF-etched (Group A), HF-etched and resin-cement (Group B) and Y-TZP (Groups C and D)) was in contact with a 10 mm diameter ring-support. The sample thickness was measured before and after testing using a digital micrometer (Mitutoyo Corporation, Tokyo, Japan) accurate to 0.01 mm. A bi-layer analytical solution was used to calculate the BFS [26]. For the uncoated specimens (Group A) and resin-coated specimens (Group B) the thickness term of the lowermost layer was inputted as zero and consequently the solution simplifies to the monolayer BFS solutions described by Shetty [27]. For the bilayered specimens groups C and D, the validity that the approximation of the contribution of the cement thickness is negligible in the bending solution has previously been demonstrated [28]. The neutral plane (t_n) was therefore calculated as a function of the veneer-ceramic and Y-TZP thicknesses (t_1 and t_2,) and elastic moduli (E_1 (64 GPa)[29] and E_2 (209.3 GPa)[30]), respectively where:

$$t_n = \frac{E_1^*(t_1)^2 - E_2^*(t_2)^2}{2(E_1^* t_1 + E_2^* t_2)} \quad \text{Eq 1.1}$$

and

$$E^* = \frac{E}{1-\nu^2} \quad \text{Eq 1.2}$$

The bi-axial flexure stresses were calculated at axial positions (z) at the centre of the disc-shaped specimens, where the bonded interface was located at $z=0$, the veneer-ceramic surface at $z=t_1$ and the Y-TZP surface at $z=-t_2$.

$$\sigma = \frac{-3P(1+\nu)(z-t_n)}{2\pi(t_1+t_2)^3}\left[1+2\ln\left(\frac{a}{b}\right)+\frac{1-\nu}{1+\nu}\left(1-\frac{b^2}{2a^2}\right)\frac{a^2}{R^2}\right]\left[\frac{E_1^*\left(E_1^* t_1 + E_2^* t_2\right)(t_1+t_2)^3}{\left(E_1^* t_1^2\right)^2 + \left(E_2^* t_2^2\right)^2 + 2E_1^* E_2^* t_1 t_2\left(2t_1^2 + 2t_2^2 + 3t_1 t_2\right)}\right] \quad \text{Eq 1.3}$$

$(0 \le z \le t_1)$ and

$$\sigma = \frac{-3P(1+\nu)(z-t_n)}{2\pi(t_1+t_2)^3}\left[1+2\ln\left(\frac{a}{b}\right)+\frac{1-\nu}{1+\nu}\left(1-\frac{b^2}{2a^2}\right)\frac{a^2}{R^2}\right]\left[\frac{E_2^*\left(E_1^* t_1 + E_2^* t_2\right)(t_1+t_2)^3}{\left(E_1^* t_1^2\right)^2 + \left(E_2^* t_2^2\right)^2 + 2E_1^* E_2^* t_1 t_2\left(2t_1^2 + 2t_2^2 + 3t_1 t_2\right)}\right] \quad \text{Eq 1.4}$$

$(-t_2 \le z \le 0)$ and

$$\nu = \frac{\left(\nu_1 t_1 + \nu_2 t_2\right)}{t_1 + t_2} \quad \text{Eq 1.5}$$

P was the load at fracture, ν_1 and ν_2 were the Poisson's ratios of the veneer-ceramic (0.25) [29] and Y-TZP (0.31) [31], respectively. a and R were the radii of the knife-edge support and specimen, respectively. b was the radius of the contact loading region and calculated according to Eq. 1.6 [27].

$$b = \frac{t_1 + t_2}{3}$$

Comparisons between the mean BFS of individual groups were made using one-way ANOVA and post-hoc Tukey tests at a 95% significance level.

Fractography

Fracture fragments generated during BFS testing were imaged using scanning electron microscopy (SEM –Zeiss EVO, Carl Zeiss GmbH, Jena, Germany). Fracture surfaces were studied qualitatively to give insight into the location of the fracture origin and sequence of fracture events. Fractographic landmarks including hackles and Wallner's lines were utilised to track the propagating crack to an initiating origin. All low strength and high strength outlying specimens were studied alongside samples representative of the mean BFS values.

Finite Element Analysis

The experimental ball-on-ring test was simulated using Finite Element Analysis (FEA). A three-dimensional finite element model of the conventional Y-TZP/veneer-ceramic and the adhesively joined Y-TZP/veneer-ceramic specimens were generated using Ansys 13.0 (ANSYS Inc, Houston, TX, USA). All materials were considered as isotropic, linear and homogeneous and the same elastic constants were used as for the closed-from analytical solutions. The interfaces between layers were idealised as perfectly bonded, and the mesh was a quadratic tetrahedral element controlled by a sizing method of 0.18 mm for the veneer-ceramic and Y-TZP layers and 0.01mm for the resin-cement interface. Maximum principal stresses (MPS) were calculated for equivalent applied loads throughout the thickness of the simulated specimens.

RESULTS

Application of resin-cement to the HF-etched VM9 veneer-ceramic surface resulted in a significant increase in mean BFS from 74.8 (9.7) to 93.9 (19.5) MPa respectively (P=0.012) (Figure 2a, Table 1). Fractographic analysis of uncoated specimens correlated obvious ceramic surface defects with low BFS values. For resin-coated specimens less reinforcement was observed in specimens possessing obvious porosity at the interface between the resin-cement and ceramic (Figure 3a). In these circumstances the fracture origin was coincident with the porosity. For high BFS values, a well adapted resin-cement surface was visible and the fracture origin was either directly in the axis of loading or translated slightly radially (< 250μm) in the direction of the specimen periphery (Figure 3b).

Despite different fabrication routes no significant differences in mean thickness of the veneer-ceramic and Y-TZP were observed between groups C and D (P>0.93) (Figure 2b). Bilayer solutions were used to calculate tensile failure stresses within the veneer-ceramic layer and the fracture origins were confirmed using fractography. The BFS calculated at the fracture origin of the cemented bilayer specimens was significantly increased when compared with the conventionally sintered Y-TZP/ceramic-veneer (P<0.01) (Table 1). The distribution of the fracture strength data remained similar with comparable variances and shapes of the survival probability distributions (Figure 2b). Fractographic analysis of the fracture fragments revealed that the fracture origins were most commonly located above the interface between veneer-ceramic and Y-TZP (approx 0.05mm) for conventionally sintered specimens (Figure 3c). For resin-cemented specimens radial fracture originating at the lowermost surface of the veneer

ceramic was obvious in most cases (Figure 3d). Low strength specimens were associated with porosity within the resin-cement layer. No delamination between resin-cement and Y-TZP was observed however fracture involving delamination of the veneer-ceramic was noted.

FEA models representative of the loading conditions and sample geometries used demonstrated the generation of tensile stresses in the region where failure was observed fractographically. At an arbitrary load of 350 N (in excess of the maximum load measured during BFS testing) the FEA predicts that the MPS generated within the Y-TZP layer remained significantly below the expected flexural strength of the material. For an identical load the MPS encountered at the lowermost surface of the veneer-ceramic (in contact with Y-TZP or resin-cement) were increased for the adhesively bonded Y-TZP/veneer-ceramic specimens and the predicted stressing pattern in this region was considered as more deleterious (Figure 4).

DISCUSSION

A bi-axial flexure geometry was chosen to measure the stress required to initiate fracture within the regions of the veneer-ceramic that are influenced by both interfacial and residual stress variables (defined for the purpose of this study as being at or immediately above the Y-TZP/veneer-ceramic interface but discretely away from the loading contact). Material constants (elastic modulus, Poisson's ratio) for Y-TZP and for a veneer-ceramic were used to populate closed form analytical solutions for ball-on-ring bending of disc-shaped bilayers (Eq 1.1-1.5) [26]. A maximum threshold load for monotonic testing of 400 N was considered as representative of masticatory loading patterns encountered clinically [32]. A 0.7 mm veneer-ceramic layer thickness was clinically relevant and the Y-TZP layer thickness was adjusted iteratively until the predicted critical tensile stresses for the veneer-ceramic could be generated at or above the Y-TZP/veneer-ceramic interface. The resultant desired Y-TZP layer thickness of 0.27 mm ensured stressing patterns within the veneer-ceramic were appropriate to test the experimental hypothesis whilst at the same time ensuring that tensile failure at the anticipated loads could not generate flexure stresses likely to cause tensile failure within the Y-TZP layer itself. The intention of the current study was not to directly replicate clinical failure where fracture can include crack extension from close to the loading or sliding load contacts [31]. In contrast, the methodology was designed to quantitatively explore how differences in residual stress states introduced by the different processing routes of RLM and conventional Y-TZP/Veneer-ceramic systems within the veneer-ceramic bulk may influence crack propagation in regions at or close to the Y-TZP/veneer interface.

The BFS of the veneer-ceramic when tested in isolation was dominated by the condition of the surface exposed to maximum tension. Modification of the surface of glassy veneer-ceramics by HF-etching to promote adhesion to the resin-cement has been demonstrated to reduce BFS and has been attributed to the extension of existing surface defects [33]. On application of the resin-cement the significant strengthening observed (~25%) was consistent with previous investigations and was attributed to the direct interaction between the resin-cement and the critical surface defect population [23,24,28]. When porosity was present within the resin-cement at the ceramic surface a lack of reinforcement was observed. Modification of the fracture strength distribution following resin-cement coating was seen as changes in the shape of the survival probability distributions and radial translation of the fracture origin observed using fractographic examination. This modification can be explained by the variable interaction between resin-cement and surface defects which resulted in a change in the fracture origin within the defect population exposed to the maximum stressing pattern. For the adhesively bonded Y-TZP/veneer-ceramic specimens (analogous to RLM) the further changes in the distribution of the fracture strength data and in the magnitude of strengthening was attributed to further modification of the interaction between resin-cement and the veneer-ceramic or by a transposition of the failure origin to within the ceramic bulk. The latter suggestion was not supported by the fractography data which demonstrated that the failure origin in the majority of cases was at the interface between resin-cement and veneer-ceramic and that radial fracture occurred. Significantly the stressing patterns modelled using FEA predict that the maximum tensile stresses in the veneer-ceramic in RLM specimens remains at the interface with the resin-cement.

For conventionally sintered veneer-ceramic/zirconia specimens it well understood that deleterious residual stress states remain within the veneer-ceramic layer [11, 34]. In the current investigation when such stress states were not accommodated within an FE model, the analysis predicted more favourable stressing patterns within the veneer-ceramic for common loading conditions when compared with RLM specimens. However, BFS testing revealed significantly reduced fracture strengths (calculated at the fractographic origin) for this fabrication route. Fractography demonstrated that the failure origin was located above the veneer-ceramic/zirconia interface. This finding would be expected as thermally induced compressive residual stresses in the veneer-ceramic would be manifested immediately above the zirconia layer leading to reinforcement [34].

Although it is not possible within the context of the reported findings to mechanistically determine the contribution of individual elements which influence system strength it is clear that adhesive cementation in RLM offers potential to induce more favourable stress states within the veneer-ceramic and at the same time control radial crack propagation through well understood effects of resin on critical defects [22]. It is important to acknowledge that in the presence of environmental and loading conditions more representative of the oral cavity that fatigue patterns are likely to differ between the two fabrication routes and that the pattern of failure and reinforcement observed are likely to be different. Further studies are therefore essential to characterise and optimise a promising fabrication route.

REFERENCES

1. Belli R, Petschelt A, Lohbauer U. Thermal-induced residual stresses affect the fractographic patterns of zirconia-veneer dental prostheses. Journal of the Mechanical Behaviour of Biomedical Materials. 2013; **21**:167-77.
2. Bulpaki P, Taskonak B, Yan J, Mecholsky JJ Jr. Failure analysis of clinically failed all-ceramic fixed partial dentures using fractal geometry. Dental Materials. 2009; **25**:634-40.
3. Heintze SD, Rousson V. Survival of zirconia-and metal-supported fixed dental prostheses: a systematic review. International Journal of Prosthodontics. 2010; **23**:493-502.
4. Sailer I, Feher A, Filser F, Gauckler LJ, Luthy H, Hammerle CH. Five-year clinical results of zirconia frameworks for posterior fixed partial dentures. International Journal of Prosthodontics. 2007; **20**:383-8.
5. Goodacre CJ, Bernal G, Rungcharassaeng K, Kan JY. Clinical complications in fixed prosthodontics. Journal Prosthetic Dentistry. 2003; **90**:31-41.
6. Aboushelib MN, Feilzer AJ, Kleverlaan CJ. Bridging the gap between clinical failure and laboratory fracture strength tests using a fractographic approach. Dental Materials. 2009; **25**:383-91.
7. Beuer F, Schweiger J, Eichberger M, Kappert HF, Gernet W, Edelhoff D. High-strength CAD/CAM-fabricated veneering material sintered to zirconia copings--a new fabrication mode for all-ceramic restorations. Dental Materials. 2009; **25**:121-8.
8. Tinschert J, Schulze KA, Natt G, Latzke P, Heussen N, Spiekermann H. Clinical behaviour of zirconia-based fixed partial dentures made of DC-Zirkon: 3 year result. International Journal of Prosthodontics. 2008; **21**:217-22.

9. Lee JJ, Kwon JY, Bhowmick S, Lloyd IK, Rekow ED, Lawn BR. Veneers vs. core failure in adhesively bonded all-ceramic crown layers. Journal of Dental Research. 2008; **87**:363-6.

10. Mitov G, Lohbauer U, Rabbo MA, Petschelt A, Pospiech P. Investigations of subcritical crack propagation of the Empress 2 all-ceramic system. Dental Materials. 2008; **24**:267-73.

11. Taskonak B, Mecholsky JJ Jr, Anusavice KJ. Residual stresses in bilayer dental ceramics. Biomaterials. 2005; **26**:3235-41.

12. Belli R, Monteiro S Jr, Baratieri LN, Katte H, Petschelt A, Lohbauer U. A photoelastic assessment of residual stresses in zirconia-veneer crowns. Journal Dental Research. 2012; **91**:316-20.

13. Fischer J, Stawarzcyk B, Trottmann A, Hämmerle CH. Impact of thermal misfit on shear strength of veneering ceramic/zirconia composites. Dental Materials. 2009; **25**:419-23.

14. Tholey MJ, Swain MV, Thiel N. Thermal gradients and residual stresses in veneered Y-TZP frameworks. Dental Materials. 2011; **27**:1102-10.

15. Göstemeyer G, Jendras M, Dittmer MP, Bach FW, Stiesch M, Kohorst P. Influence of cooling rate on zirconia/veneer interfacial adhesion. Acta Biomaterialia. 2010. **6**:4532-8.

16. Benetti P, Kelly JR, Sanchez M, Della Bona A. Influence of thermal gradients on stress state of veneered restorations. Dental Materials. 2014; **30**:554-63

17. Cheng X, Fisher JW, Prask HJ , Gnaupel-Herold T, Ben TY, Roy S. Residual stress modification by post-weld treatment and its beneficial effect on fatigue strength of welded structures. International Journal of Fatigue. 2003; **25**:1259–1269.

18. Kurbad A. Digital veneering 2 -fabrication of CAD/CAM veneer structures with Rapid Layer Technology. International Journal of Computerised Dentistry. 2011; **14**:343-52.

19. Schmitter M1, Mueller D, Rues S. Chipping behaviour of all-ceramic crowns with zirconia framework and CAD/CAM manufactured veneer. Journal of Dentistry. 2012; **40**:154-62.

20. Wiedhahn K. The impression-free Cerec multilayer bridge with the CAD-on method. International Journal of Computerised Dentistry. 2011;**14** :33-45.

21. Schmitter M, Mueller D, Rues S. In vitro chipping behaviour of all-ceramic crowns with a zirconia framework and feldspathic veneering: comparison of CAD/CAM-produced veneer with manually layered veneer. Journal of Oral Rehabilitation. 2013; **40**:519-25.

22. Lee JJ-W, Lloyd IK, Chai H, Jung Y-G, Lawn BR. Arrest, deflection, penetration and reinitiation of cracks in brittle layers across adhesive interlayers. Acta Materialia. 2007; **55**:5859-66.

23. Addison O, Marquis PM, Fleming GJ. Adhesive luting of all-ceramic restorations--the impact of cementation variables and short-term water storage on the strength of a feldspathic dental ceramic. Journal of Adhesive Dentistry. 2008; **10**:285-93.

24. Addison O, Marquis PM, Fleming GJ. Resin elasticity and the strengthening of all-ceramic restorations. Journal of Dental Research. 2007; **86**:519-23.

25. Fleming GJ, Jandu HS, Nolan L, Shaini FJ. The influence of alumina abrasion and cement lute on the strength of a porcelain laminate veneering material. Journal of Dentistry. 2004; **32**:67-74.

26. Hsueh CH, Lance MJ, Ferber MK. Stress Distributions in thin bilayer discs subjected to ball-On-ring Tests. Journal of the American Ceramic Society. 2005; **88**: 1687–1690.

27. Hsueh CH, Luttrell CR, Becher PF. Modelling of bonded multilayered disks subjected to biaxial flexure tests. International Journal of Solids and Structures. 2006; **43**: 6014–6025.

28. Addison O, Fleming GJ. Application of analytical stress solutions to bi-axially loaded dental ceramic-dental cement bilayers. Dental Materials. 2008; **24**:1336-42.

29. Zeng K, Odén A, Rowcliffe D. Evaluation of mechanical properties of dental ceramic core materials in combination with porcelains. International Journal of Prosthodontics. 1998; **11**:183-9.

30. Borba M, de Araújo MD, de Lima E, Yoshimura HN, Cesar PF, Griggs JA, Della Bona A. Flexural strength and failure modes of layered ceramic structures. Dental Materials. 2011; **27**:1259-66.

31. Kim JW, Liu L, Zhang Y. Improving the resistance to sliding contact damage of zirconia using elastic gradients. Journal Biomedical Materials Research, Part B Applied Biomaterials. 2010; **94**:347-52.

32. Rekow D, Thompson VP. Engineering long term clinical success of advanced ceramic prostheses. Journal of Material Science Materials in Medicine. 2007; **18**:47-56.

33. Addison O, Marquis PM, Fleming GJ. The impact of hydrofluoric acid surface treatments on the performance of a porcelain laminate restorative material. Dental Materials. 2007; **23**:461-8

34. Fukushima KA, Sadoun MJ, Cesar PF, Mainjot AK. Residual stress profiles in veneering ceramic on Y-TZP, alumina and ZTA frameworks: measurement by hole-drilling. Dental Materials. 2014; **30**:105-11.

FIGURES

Figure 1. Schematic diagrams of the representative specimen geometries of Groups A-D. Figures are not drawn to scale.

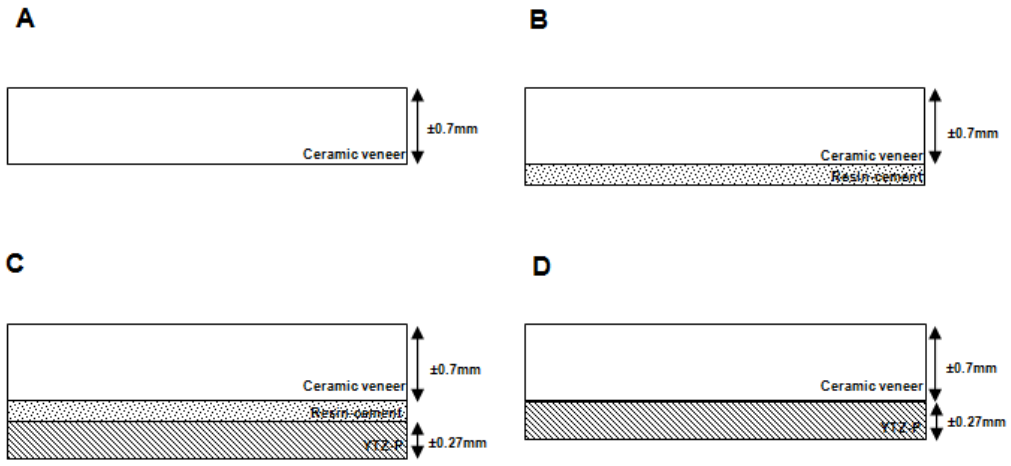

Figure 2: **(a)** Plot of bi-axial flexure strength against survival probability for monolithic veneer-ceramic disc-shaped specimens measured before (Group A) and after resin-cement application (Group B). **(b)** Plot of bi-axial flexure strength against survival probability for bilayered Y-TZP/veneer-ceramic disc-shaped specimens prepared by mimicking Rapid Layer Manufacture (RLM) by adhesive bonding the veneer-ceramic to the Y-TZP (Group C) or by conventional veneer-ceramic sintering (Group D)

(2a)

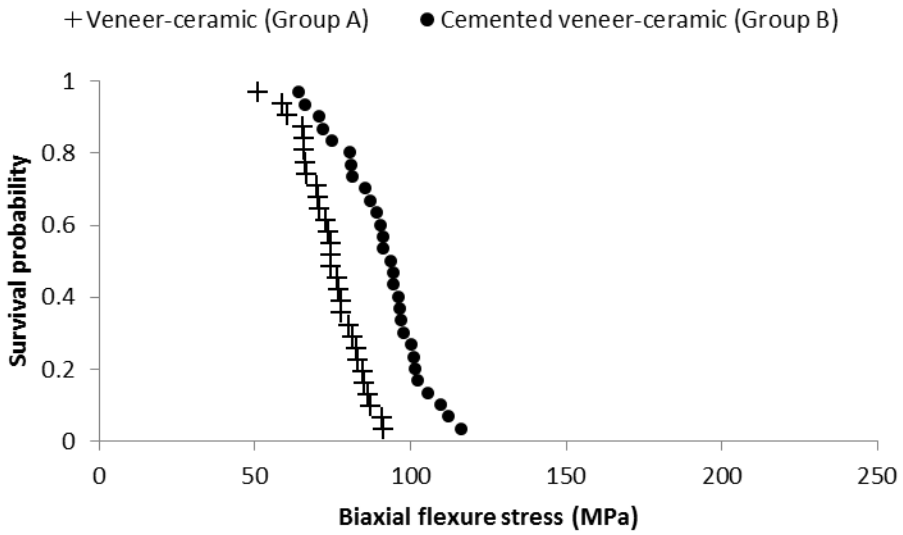

(2b)

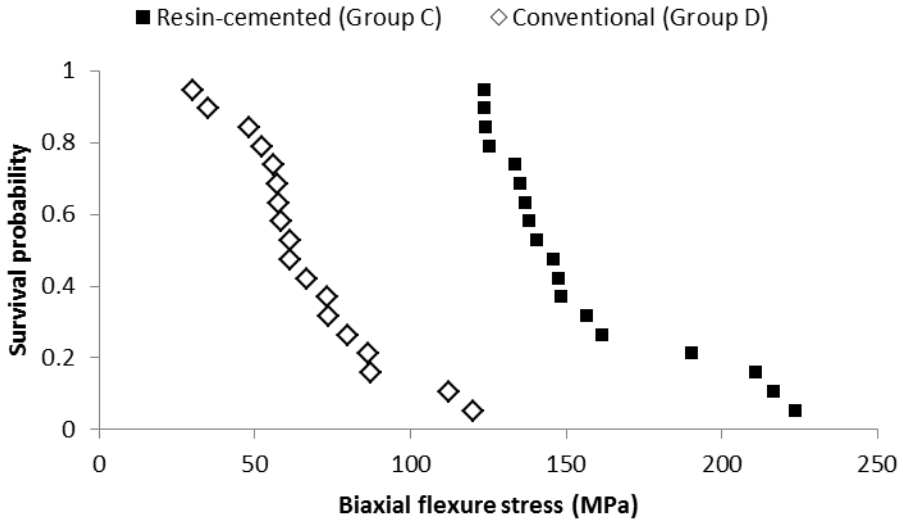

Figure 3: Scanning electron micrographs of fracture surfaces of disc-shaped ceramic specimens following BFS determination. **(3a)** demonstrates a low strength resin-cement coated veneer-ceramic specimen (Group B) where there is clear porosity within the adhesive and the fracture origin is closely associated. **(3b)** demonstrates a high strength resin-cement coated veneer-ceramic specimen (Group B) where the resin-cement is intimately associated with the lowermost surface of the veneer-ceramic. **(3c)** demonstrates a conventionally sintered Y-TZP/veneer-ceramic bilayer (Group D) where the fracture origin can be traced to above the Y-TZP/veneer-ceramic interface. Damage from near the contact loading site is evident but was determined as a secondary event at the fracture features are shown to bisect wake hackles formed from the initial fracture event. **(3d)** demonstrates clear radial fracture of the veneer-ceramic observed in the Rapid Layer Manufacture (RLM) mimicking bilayer specimens (Group C) and was observed in the majority of cases. Low strength specimens were associated with porosity within the resin-cement layer. For bi-layered specimens Y-TZP fracture observed in **3c,d** occurred after the initial fracture event.

(a)

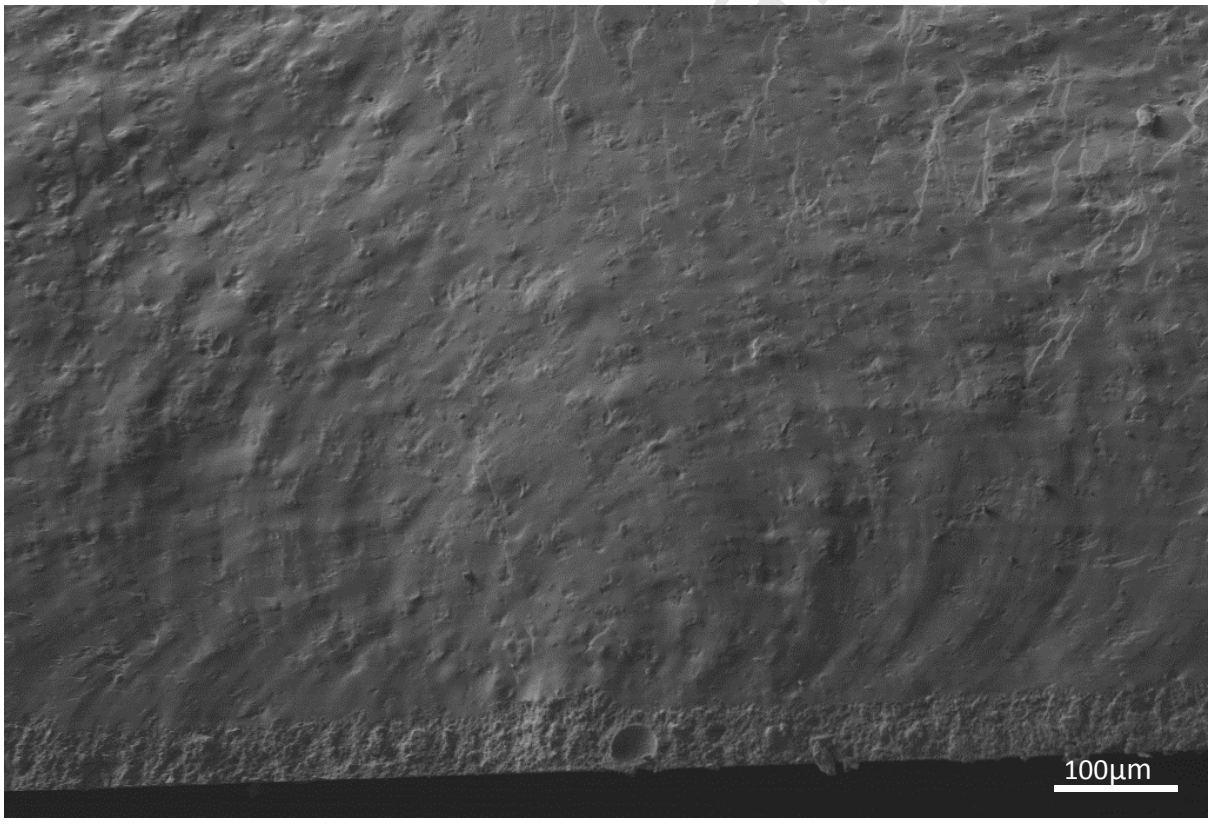

(b)

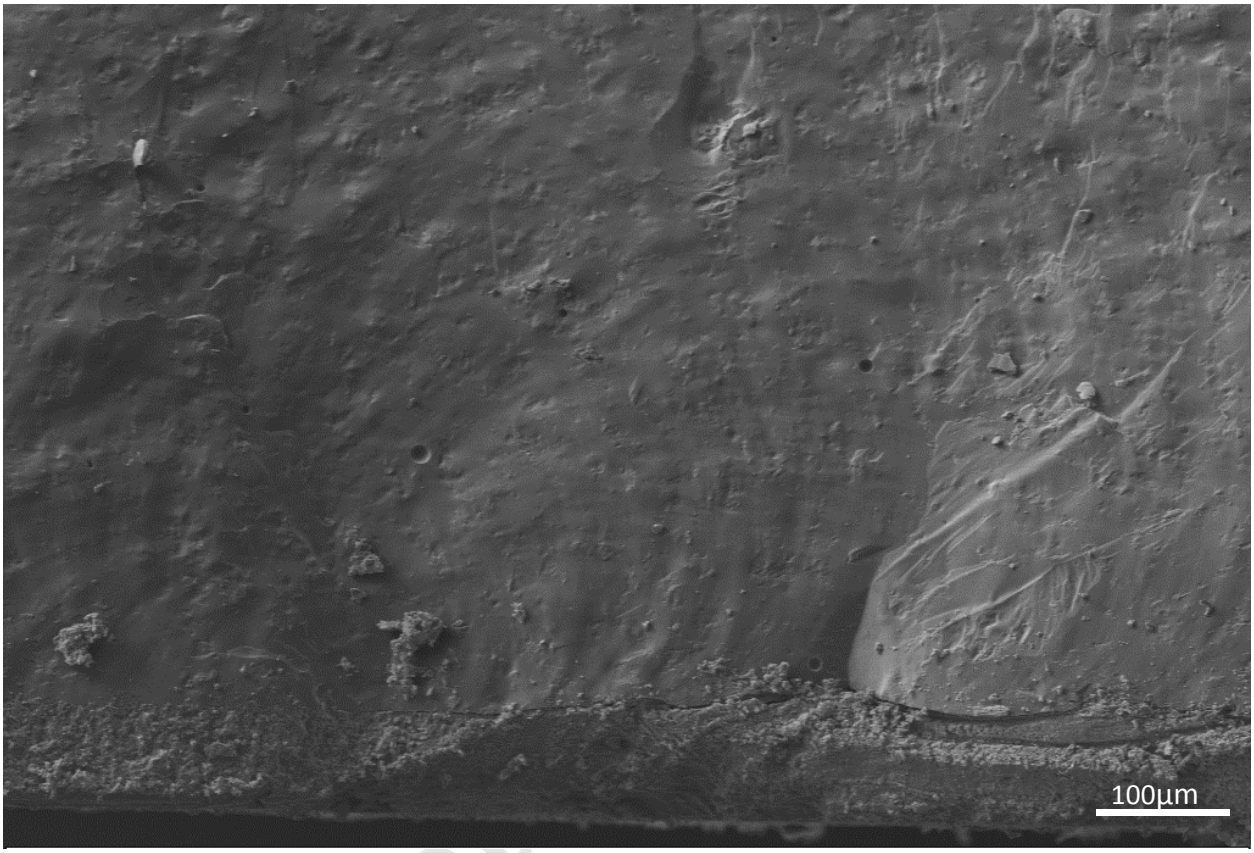

(c)

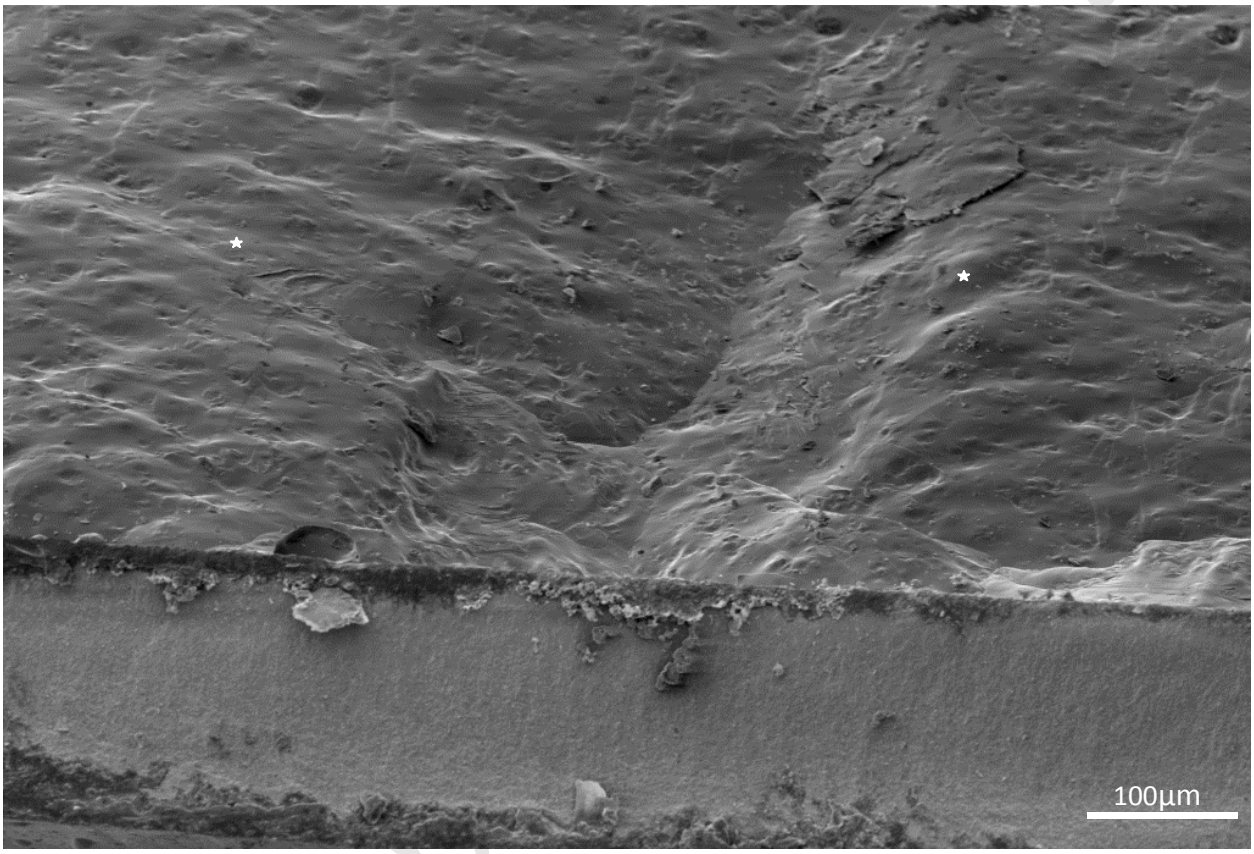

(d)

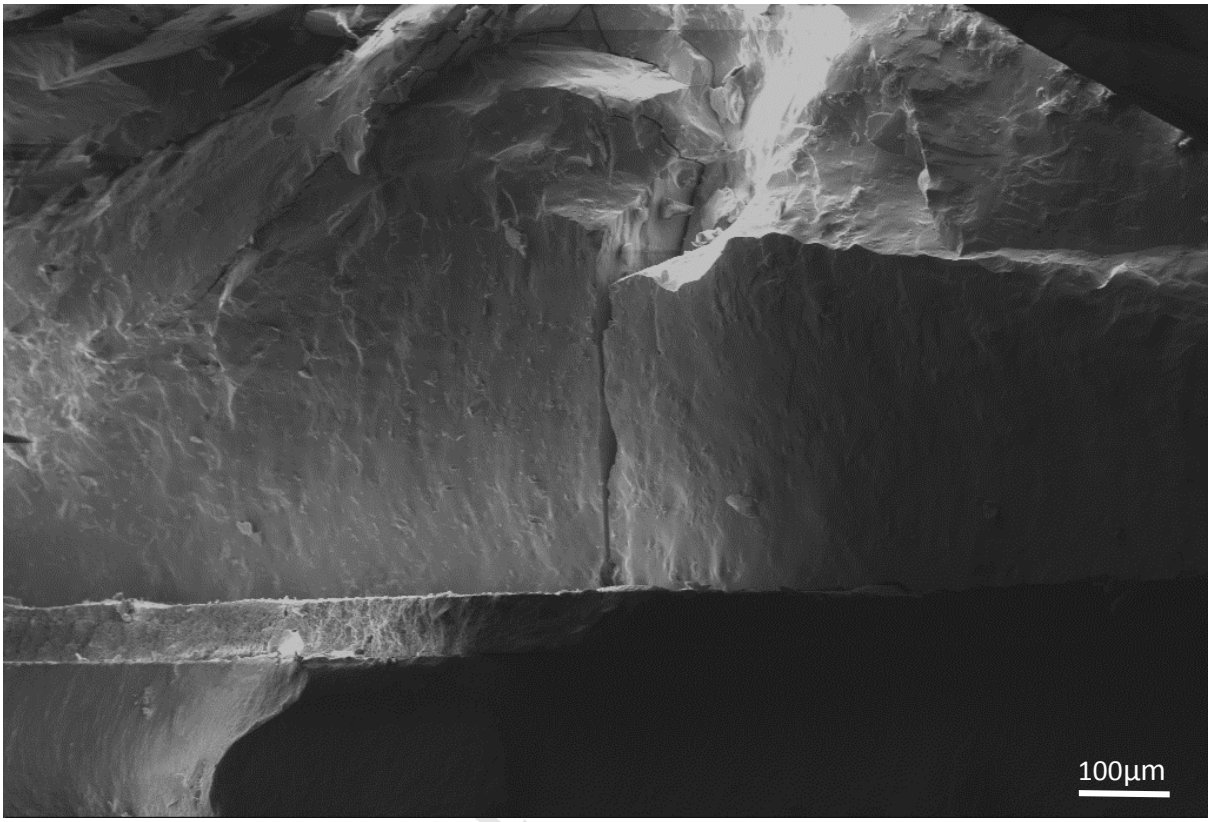

Figure 4: A maximum principal stress contour plot for the bilayer conditions modelled using a nominally identical load of 350 N (which exceeded the maximum loading conditions encountered experimentally). For conventionally sintered bilayers (a) tensile stresses were predicted at the interface and the Maximum Principle Stress (MPS) in the Y-TZP layer was below the predicted flexure strength of this material. For Rapid Layer Manufacture (RLM) mimicking bilayer specimens (b) increased tensile stresses were predicted at the lowermost surface of the veneer-ceramic when in contact with the ring-support.

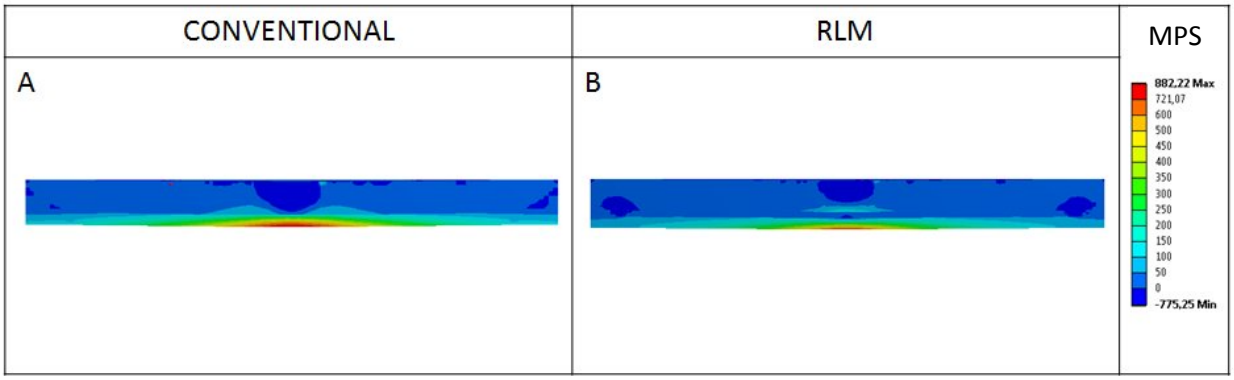

TABLES:

Table 1: The mean failure load (N) and Bi-axial Flexure Strength (BFS) calculated at the fracture origin (MPa) (Group A), resin-coated veneer-ceramic (Group B), adhesively bonded Y-TZP/veneer-ceramic bilayer (Group C) and conventionally sintered Y-TZP/veneer-ceramic bilayer (Group D) specimens. Numbers in parantheses refer to standard deviations. Common superscripts refer to non-significant differences between paired groups identified through one-way ANOVA and post-hoc Tukey tests ($\alpha = 0.05$).

Group	**A**	**B**	**C**	**D**
Mean Failure Load (N)	29.1 (4.5)	35.5 (6.0)	248.2 (58.8)	197.7 (62.9)
Mean BFS (MPa)	74.8 (9.7)[a]	93.9 (19.5)[b]	154.7 (33.0)[c]	67.6 (23.4)[a]
BFS range (MPa)	51.2-91.4	64.2-170.6	123.9-223.8	30.1-120.3

ACKNOWLEDGMENT

Dr Anna Costa is supported by CAPES - Coordenação de Aperfeiçoamento de Pessoal de Nível Superior.